Reports

Scanning Tunneling Microscopy of Freeze-Fracture Replicas of Biomembranes

JOSEPH A. N. ZASADZINSKI, JASON SCHNEIR, JOHN GURLEY, VIRGIL ELINGS, PAUL K. HANSMA

The high resolution of the scanning tunneling microscope (STM) makes it a potentially important tool for the study of biomaterials. Biological materials can be imaged with the STM by a procedure in which fluid, nonconductive biomaterials are replaced by rigid and highly conductive freeze-fracture replicas. The three-dimensional contours of the ripple phase of dimyristoylphosphatidylcholine bilayers were imaged with unprecedented resolution with commercial STMs and standard freeze-fracture techniques. Details of the ripple amplitude, asymmetry, and configuration unobtainable by electron microscopy or x-ray diffraction can be observed relatively easily with the STM.

THE SCANNING TUNNELING MICROscope (STM), developed by Binnig *et al.* (*1*), is one of the most important recent advances in surface analytical instrumentation (*2–4*). A goal of many research groups is to apply the superior resolving power of the STM to biomaterials. Sonnenfeld and Hansma have used the STM to produce high-resolution images of crystalline solids in water (*5*); Smith *et al.* have imaged ordered Langmuir-Blodgett films of cadmium arachidate (*6*). A limited number of biological macromolecules have been imaged with the STM, including DNA in vacuum (*7*), metal-shadowed DNA (*8*), DNA in water (*9*), a globular protein (*10*), bacteriophage ϕ29 (*11*), and porin vesicles (*12*), but with limited resolution. Difficult limitations must be overcome before biomembranes and other structured fluids can be routinely imaged with the STM. The first of these is that most biological materials are extremely poor conductors. To overcome this limitation, Binnig *et al.* (*13*) introduced the atomic force microscope (AFM). This microscope features a tip mounted on a small, cantilevered beam. The interatomic forces between the tip and the sample deflect the cantilever, and this deflection is monitored. Using the AFM, Marti *et al.* (*14*) have imaged polymerized organic monolayers with subnanometer resolution.

The second limitation of both the STM and the AFM is that fluid samples are easily deformed (the crystalline solids that are usually imaged are not readily deformed). In phospholipid membranes, Brownian motion and other thermal fluctuations can be large, often much larger than the features of interest. If the thermal motions are quenched by rapid freezing, it might be possible to image the sample with a low-temperature AFM (such a device has yet to be perfected), or, as we show here, the low-temperature surface can be replaced with a platinum-carbon replica by conventional freeze-fracture techniques. A commercial STM can then be used to image the surface at ambient temperature and pressure.

An excellent candidate for freeze-fracture STM is the $P_{\beta'}$ or ripple phase of dimyristoylphosphatidylcholine (DMPC) bilayers. The $P_{\beta'}$ phase is one of the most studied, yet still poorly understood, biomembrane structures (*15–19*) (Fig. 1). In DMPC, the headgroup area is large compared to the area occupied by the fully extended, frozen chains at temperatures below the main phase transition (*15–19*). Below about 14°C, DMPC in water forms an $L_{\beta'}$ phase, in which the chains are tilted with respect to the bilayer normal and the lamellae are flat (*15–18*). Above the main transition temperature of roughly 24°C, the hydrocarbon chains melt, the head group and tail group areas are better balanced, the bilayers are smooth and flat, and the DMPC molecules are normal to the layers; this structure is called the L_α phase. In the $P_{\beta'}$ phase, from 14° to 24°C, DMPC bilayers exhibit regular, three-dimensional intrabilayer corrugations, hence the name ripple phase. The rippling in the $P_{\beta'}$ phase is believed to be an alternative way of satisfying the head-tail area incompatibility (*19*).

X-ray diffraction (*15, 16*) and freeze-fracture replication transmission electron microscopy (TEM) (*17, 18*) have been the primary experimental tools used to study the structure of the ripples in the $P_{\beta'}$ phase and in biomembranes in general. With both techniques the predominant wavelength of the fully hydrated DMPC ripples is between 12 and 13 nm (*10–14*). Estimates of the ripple height range from 0.8 to 8 nm (*15, 17, 18, 20*), and the ripple configuration is undetermined. Imaging freeze-fracture replicas of DMPC ripples with the STM can remove much of this ambiguity, and the combined techniques have the potential to greatly broaden the applications of the STM.

Crystalline $L-\alpha$ DMPC of reported 99%$^+$ purity (Sigma, St. Louis) was mixed with sufficient doubly distilled water to form a mixture of 65% DMPC by weight. The mixture was gently shaken and was then kept at a temperature of 35°C for several hours to induce complete swelling of DMPC with water. The sample temperature was then lowered to 18° ± 1°C (approximately the midrange of the $P_{\beta'}$ phase), and layers (10 to 50 μm thick) between two copper planchettes (Balzers BUO-12-056T; Hudson, New Hampshire) were quickly frozen by immersion in liquid propane, cooled by liquid nitrogen to −190°C (*17, 18, 21*). The specimens for STM were fractured at −170°C and 10^{-8} torr in a Reichert-Jung Cryofract 190 freeze-fracture device (Cambridge Instruments, Buffalo, New York) and immediately replicated with 2.5 nm of a platinum-carbon mixture applied by electron beam evaporation normal to the fracture surface, followed by a 30-nm reinforcing film of carbon, also applied at normal incidence. Biomembranes are known to fracture preferentially along the hydrocarbon interior of the bilayers (*22*). Samples for TEM were prepared in a similar fashion, except that a 1.0-nm platinum-carbon layer was applied at a 45° angle to the fracture surface. The replica films were freed from the copper planchettes, cleaned as described elsewhere (*18*), and mounted on 500-mesh gold electron microscope grids (Pelco, Tustin, California). The replicas were oriented so that the side directly contacting the sample surface was imaged by the STM. TEM images, recorded with a JEOL 100 CX-II instrument, revealed extensive areas of rippled DMPC bilayers of wavelength 12 ± 0.5 nm, in good agreement with published results (*15–17*), indicating that the freezing and replication were satisfactory (Fig. 1A).

Commercially available STMs were used in this study (Digital Instruments, Goleta, California). Images were obtained in the

J. A. N. Zasadzinski, Department of Chemical and Nuclear Engineering, University of California, Santa Barbara, CA 93106.
J. Schneir, V. Elings, P. K. Hansma, Department of Physics, University of California, Santa Barbara, CA 93106.
J. Gurley, Digital Instruments Inc., Goleta, CA 93117.

constant current mode (*4*) at ambient temperature and pressure. The transverse calibration of the microscopes was established by imaging the well-known surface of graphite. The vertical calibration was obtained by recording the change in piezoelectric voltage necessary to move the tip a known distance (one step of a stepper motor). STM images were recorded by photographing either a storage oscilloscope screen (Fig. 1B) or a computer monitor (Fig. 1, C and D). The lines are z versus x plots separated by Δy. The tunneling tips used were commercially available electrochemically etched platinum-iridium microelectrodes (Fig. 1B) (Longreach Scientific Resources; Orr's Island, Maine) or mechanically formed platinum-iridium tips (Fig. 1, C and D) (Digital Instruments). The x scan rate was ≈22 Hz, and the tunneling current was 2.5 nA (Fig. 1B) or 1.0 nA (Fig. 1, C and D). For imaging, a bias voltage of +1.0 V was used for Fig. 1B and 20 mV for Fig. 1, C and D, with the sample positive with respect to the tip. The replica, on its gold support, was firmly mounted to a glass cover slip with cyanoacrylate to minimize the effect of vibrations. A metal clip then served the dual function of firmly holding the gold support and cover glass against the STM base and making electrical contact.

Figure 1B shows an image of the replica surface taken with an analog STM (Nanoscope I) with no y scan. The spacing between the rows is 13 nm, in good agreement with published values (*15–18*), and the height is about 4.5 nm. As Fig. 1B was taken, the x scan speed was increased from 15 to 30 Hz. Thus Fig. 1B shows that the height, spacing, and position of the rows are independent of scan speed for the slower scans. The ripple configuration is somewhat asymmetric, rising more steeply on the left than on the right, in agreement with TEM results (*17, 18*). The ripples appear smooth with no sharp corners. Figure 1, C and D, shows higher magnification views taken with a newer digital STM (Nanoscope II). As with most advances in instrumentation, old questions are answered and new ones arise. In this case, the old questions about ripple depth and asymmetry are answered. The new questions include: (i) What is the significance of the periodicity seen along each ripple? (ii) Is it molecular structure, an artifact of the replica process, or something else? Further research, including measurements of the change in tunneling current with change in tip height (*9*), may help in finding any organic residues on the replica surface. This information could lead to important refinements in preparing and cleaning replicas for examination in the STM.

In conclusion, a commercial STM can be teamed with conventional freeze-fracture replication techniques to provide high-resolution, three-dimensional images of biological membranes and other structured fluids and liquid crystals. The preliminary images presented here show that the ripples in the $P_{\beta'}$ phase of DMPC are slightly asymmetric and smoothly varying, except for a previously unobserved, regular banding roughly orthogonal to the ripple direction. The peak-to-trough height is about 4.5 nm, which from previous experimental and theoretical work appears reasonable. Metal freeze-fracture replicas of biomembranes eliminate much of the difficulty in imaging biomaterials and can greatly enlarge the type and number of surfaces that can be examined with the STM.

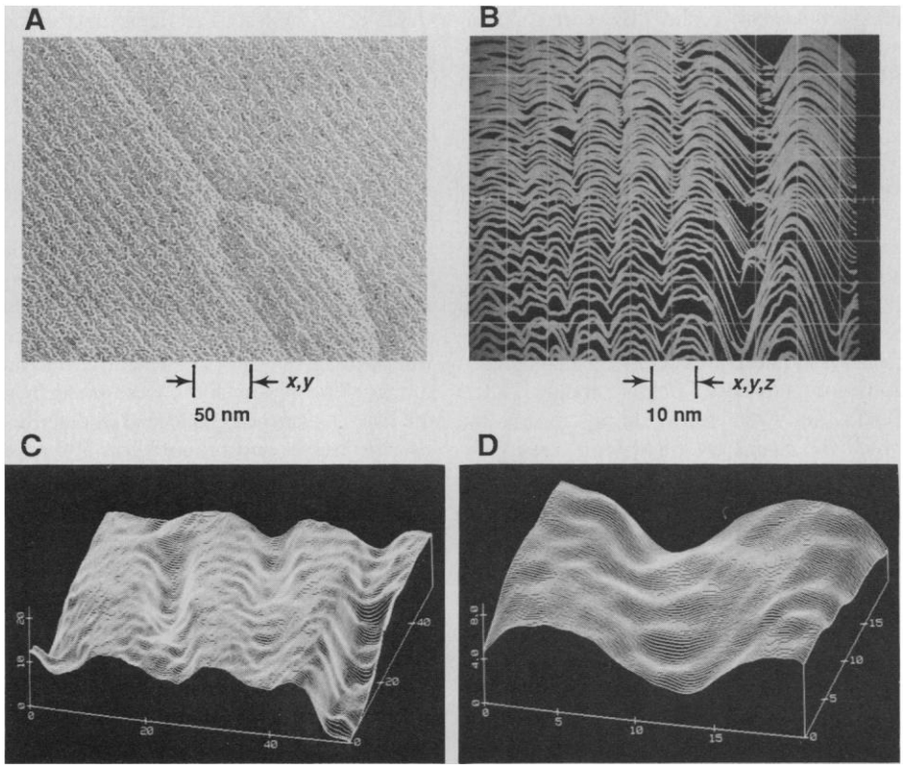

Fig. 1. (**A**) Transmission electron micrograph of a freeze-fracture replica of the $P_{\beta'}$ phase of DMPC. Ripple periodicity is about 12 nm. Ripples are often interrupted by defects, such as the screw dislocation line that passes through this image. (**B**) Analog STM image of the replica with no y scan. Scan speed is increased from 15 Hz (bottom) to 30 Hz (top). Although detail is washed out in the fastest scans, the essential features are clear: (i) ripple periodicity is 13 nm and average amplitude is 4.5 nm and (ii) the ripples are asymmetric, rising more steeply to the left than to the right. (**C**) Digital STM image of the replica. The ripple amplitude and configuration are well defined as in (B), although variations occur along the ripple. Note the fine structure that crosses the ripples roughly orthogonal to the ripple direction. The distance scale is in nanometers. (**D**) Computer zoom of the right-central portion of (C). The bands crossing the ripples are readily apparent. At present, it is difficult to say if the banding reflects an underlying molecular structure of the ripple phase, a structure inherent to the replica itself, or some unknown artifact.

REFERENCES AND NOTES

1. G. Binnig, H. Rohrer, Ch. Gerber, E. Weibel, *Phys. Rev. Lett.* **49**, 57 (1982).
2. For recent reviews see G. Binnig and H. Rohrer, *Sci. Am.* **253**, 50 (August 1985); C. F. Quate, *Phys. Today* **39**, 26 (1986).
3. J. A. Golovchenko, *Science* **232**, 48 (1986).
4. P. K. Hansma and J. Tersoff, *J. Appl. Phys.* **61**, R1 (1987).
5. R. Sonnenfeld and P. K. Hansma, *Science* **232**, 211 (1986).
6. D. P. E. Smith *et al.*, *Proc. Natl. Acad. Sci. U.S.A.* **84**, 969 (1987).
7. G. Binnig and H. Rohrer, in *Trends in Physics*, J. Janta and J. Panatoflicek, Eds. (European Physical Society, Petit-Lancy, Switzerland, 1983), p. 38.
8. G. Travaglini, H. Rohrer, M. Amrein, H. Gross, *Surf. Sci.* **181**, 350 (1987).
9. S. M. Lindsay and B. Barris, *J. Vac. Sci. Technol. A*, in press.
10. D. Dahn, W. Watanabe, B. Blackford, M. H. Jericho, *ibid.*, in press.
11. A. M. Baró *et al.*, *Nature (London)* **315**, 253 (1985).
12. A. O. Stemmer *et al.*, *Surf. Sci.* **181**, 294 (1987).
13. G. Binnig, C. F. Quate, Ch. Gerber, *Phys. Rev. Lett.* **56**, 930 (1986).
14. O. Marti *et al.*, *Science* **239**, 50 (1988).
15. A. Tardieu, V. Luzzatti, F. C. Reman, *J. Mol. Biol.* **75**, 711 (1973); M. J. Janiak, D. M. Small, G. G. Shipley, *J. Biol. Chem.* **254**, 6068 (1979).
16. G. S. Smith, C. R. Safinya, D. Roux, N. A. Clark, *Mol. Cryst. Liq. Cryst.* **144**, 235 (1987).
17. E. J. Luna and H. M. McConnell, *Biochim. Biophys. Acta* **466**, 381 (1977); D. Rüppel and E. Sackmann, *J. Phys. (Paris)* **44**, 1025 (1983).
18. J. A. N. Zasadzinski and M. B. Schneider, *J. Phys. (Paris)* **48**, 2001 (1987).
19. S. Doniach, *J. Chem. Phys.* **70**, 4587 (1979); P. A. Pearce and H. L. Scott, *ibid.* **77**, 951 (1982); M. S. Falkovitz, M. Seul, H. L. Frisch, H. M. McConnell, *Proc. Natl. Acad. Sci. U.S.A.* **79**, 3918 (1982); J. M. Carlson and J. P. Sethna, *Phys. Rev. A*, in press.
20. R. Krbecek, C. Gebhardt, H. Gruler, E. Sackmann,

Biochim. Biophys. Acta **554**, 1 (1979).
21. M. J. Costello and J. M. Corless, *J. Microsc. (Oxford)* **112**, 17 (1978); T. Gulik-Krzywicki and M. J. Costello, *ibid.*, p. 103.
22. D. Branton, *Proc. Natl. Acad. Sci. U.S.A.* **55**, 1048 (1966).
23. We thank D. W. Berreman and M. J. Sammon for valuable discussions on the possibility of imaging freeze-fracture replicas with the STM; R. Coleman for his collaboration on preliminary experiments with replicas; H. Ribi, W. Stoekenius, and S. Lindsay for stimulating discussions on the importance of imaging biological samples with the STM; J. Israelachvili for continuing discussions on the relation between membrane structure and function; C. Bracker for helpful suggestions and improvements to the manuscript; and J. Reynolds for typing. J.A.N.Z. is supported by Petroleum Research Foundation grant 18915-G7 and NSF Presidential Young Investigator Award CBT86-57444. J.S. and P.K.H. are supported by NSF grant DMR86-13486.

19 October 1987; accepted 26 January 1988

A New High-Temperature Superconductor: $Bi_2Sr_{3-x}Ca_xCu_2O_{8+y}$

M. A. SUBRAMANIAN, C. C. TORARDI, J. C. CALABRESE, J. GOPALAKRISHNAN, K. J. MORRISSEY, T. R. ASKEW, R. B. FLIPPEN, U. CHOWDHRY, A. W. SLEIGHT

A new superconductor that displays onset behavior near 120 K has been identified as $Bi_2Sr_{3-x}Ca_xCu_2O_{8+y}$ with x ranging from about 0.4 to 0.9. Single crystal x-ray diffraction data were used to determine a pseudo-tetragonal structure based on an A-centered orthorhombic subcell with a = 5.399 Å, b = 5.414 Å, and c = 30.904 Å. The structure contains copper-oxygen sheets as in La_2CuO_4 and $YBa_2Cu_3O_7$, but the copper-oxygen chains present in $YBa_2Cu_3O_7$ do not occur in $Bi_2Sr_{3-x}Ca_xCu_2O_{8+y}$. The structure is made up of alternating double copper-oxygen sheets and double bismuth-oxygen sheets. There are Ca^{2+} and Sr^{2+} cations between the adjacent Cu-O sheets; Sr^{2+} cations are also found between the Cu-O and Bi-O sheets. Electron microscopy studies show an incommensurate superstructure along the a axis that can be approximated by an increase of a factor of 5 over the subcell dimension. This superstructure is also observed by x-ray diffraction on single crystals, but twinning can make it appear that the superstructure is along both a and b axes. Flux exclusion begins in our samples at about 116 K and is very strong by 95 K. Electrical measurements on a single crystal of $Bi_2Sr_{3-x}Ca_xCu_2O_{8+y}$ show a resistivity drop at about 116 K and apparent zero resistivity at 91 K.

MICHEL *ET AL.* (*1*) REPORTED SUperconductivity in the Bi/Sr/Cu/O system with a transition temperature (T_c) in the 7 to 20 K range. Although they presented some unit cell dimensions, they did not report a structure for the compound they designated as $Bi_2Sr_2Cu_2O_{7+y}$. On 22 January 1988, there was a report from Maeda *et al.* (*2*) that a T_c onset near 120 K can be obtained in the Bi/Sr/Ca/Cu/O system. This result was immediately reproduced by others (*2*). Chu and coworkers (*2*) subsequently announced superconductivity in the Bi/Sr/Ca/Cu/Al/O system but indicated that the Al was not important. Although some characterization of phases in the Bi/Sr/Ca/Cu/O system has been reported (*3*), none of the structures of the various phases in the system have been revealed. We have explored these systems and discovered a superconducting phase best described as $Bi_2Sr_{3-x}Ca_xCu_2O_{8+y}$.

Many compositions (about 300) in the Bi/Sr/Ca/Cu/O system were prepared by reacting Bi_2O_3, $CaCO_3$, $SrO_2/Sr(NO_3)_2$, and CuO in various proportions at 700° to 900°C in air for 12 to 36 hours. Black, platelike, and needle-shaped crystals were found in many preparations. Flux exclusion measurements showed superconductivity around 85 to 95 K in many of the samples but never in samples prepared at 700°C. Most of our samples were slowly cooled. However, quenching the samples directly into liquid nitrogen did not lower the T_c significantly. Powder x-ray diffraction revealed that most products were multiphase containing unreacted CuO, mixed oxides of Ca, Sr, and Cu, as well as a new phase having a characteristic reflection with a d-value of ~15.4 Å in the powder pattern. The Meissner effect was particularly strong whenever the 15.4 Å d-value in the x-ray pattern was predominant. Chemical analyses on samples showing the strongest flux exclusion indicated that of the total copper present about one-third is Cu^{3+} and two-thirds is Cu^{2+}.

Single crystals of the superconducting phase were grown from a Bi:Sr:Ca:Cu = 2:2:1:3 oxide mixture in a gold crucible. The mixture was heated to 850° to 900°C, held for 36 hours and cooled at the rate of 1°C per minute. Plate-like crystals that exhibited cleavage in the basal plane were predominant in the melt. They were mechanically separated and used for further characterization and structure determination. Both flux exclusion and electrical resistivity measurements on the single crystals revealed a sharp superconducting transition at $T_c \sim 95$ K (Figs. 1 and 2). In these single crystals the T_c onset occurs at about 116 K. This suggests that it is unlikely that two distinctly different structures are responsible for T_c's near 116 K and 95 K.

Single crystal x-ray diffraction information is summarized in Table 1. Many crystals show superstructure along the a and b axes, characteristic of twinning. Axial oscillation photographs of a crystal showed a super-

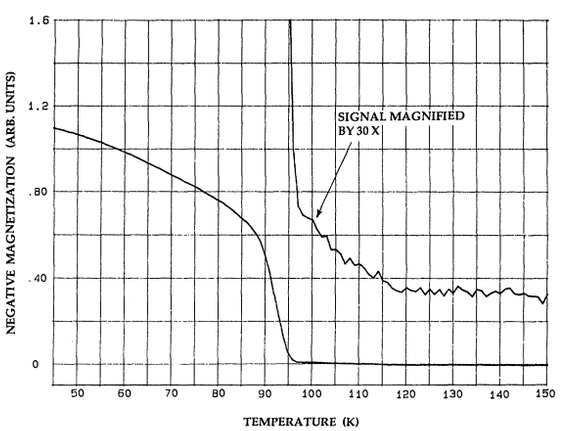

Fig. 1. Magnetic flux exclusion of a few randomly oriented single crystals of $Bi_2Sr_{3-x}Ca_xCu_2O_{8+y}$ superconductor measured by an ac susceptometer.

Central Research and Development Department, E. I. du Pont de Nemours and Company, Experimental Station, Wilmington, DE 19898.